

# End Group Dye-Labeled Polycarbonate Block Copolymers for Micellar (Immuno-)Drug Delivery

Christian Czysch, Carolina Medina-Montano, Nils-Jørgen Knudsen Dal, Thi Dinh, Yannick Fröder, Pia Winterwerber, Konrad Maxeiner, Hans-Joachim Räder, Detlef Schuppan, Hansjörg Schild, Matthias Bros, Bernhard Biersack, Federico Fenaroli, Stephan Grabbe, and Lutz Nuhn\*

Defined conjugation of functional molecules to block copolymer end groups is a powerful strategy to enhance the scope of micellar carriers for drug delivery. In this study, an approach to access well-defined polycarbonate-based block copolymers by labeling their end groups with single fluorescent dye molecules is established. Following controlled polymerization conditions, the block copolymers' primary hydroxy end group can be converted into activated pentafluorophenyl ester carbonates and subsequently aminolyzed with fluorescent dyes that are equipped with primary amines. During a solvent-evaporation process, the resulting end group dye-labeled block copolymers self-assemble into narrowly dispersed ~25 nm-sized micelles and simultaneously encapsulate hydrophobic (immuno-)drugs. The covalently attached fluorescent tracer can be used to monitor both uptake into cells and stability under biologically relevant conditions, including incubation with blood plasma or during blood circulation in zebrafish embryos. By encapsulation of the toll-like receptor 7/8 (TLR7/8) agonist CL075, immune stimulatory polymeric micelles are generated that get internalized by various antigen-presenting dendritic cells and promote their maturation. Generally, such end group dye-labeled polycarbonate block copolymers display ideal features to permit targeted delivery of hydrophobic drugs to key immune cells for vaccination and cancer immunotherapy.


## 1. Introduction

Several recently discovered pharmaceutically active compounds target highly promising cellular receptors or pathways, but have poor aqueous solubility for efficient in vivo application. To increase those drugs' bioavailability, nanometer-sized polymer particles can assist as carriers which both solubilize the compounds in water and enhance their delivery to desired site-of-actions while avoiding off-target effects.<sup>[1–5]</sup>

Especially in immunotherapy, such nanocarriers are crucial to focus the delivery of immunomodulatory drugs to restricted sites and thereby avoid unwanted toxicities through systemic immunostimulation.<sup>[6,7]</sup> Most notably, the body's immune response can be activated by addressing the innate immune system through pattern recognition receptors (PRRs). Among them, the toll-like receptors (TLRs) can effectively be stimulated by poly(I:C) (TLR3), lipopolysaccharide (LPS;TLR4), imidazoquinolines

C. Czysch, T. Dinh, Y. Fröder, P. Winterwerber, K. Maxeiner, H.-J. Räder, L. Nuhn  
 Max Planck Institute for Polymer Research Mainz  
 Ackermannweg 10, 55128 Mainz, Germany  
 E-mail: lutz.nuhn@mpip-mainz.mpg.de  
 C. Medina-Montano, M. Bros, S. Grabbe  
 Department of Dermatology  
 University Medical Center Mainz  
 Langenbeckstraße 1, 555131 Mainz, Germany

N.-J. K. Dal, F. Fenaroli  
 Department of Bioscience  
 University of Oslo  
 Blindernveien 31, Oslo 0371, Norway  
 D. Schuppan  
 Institute of Translational Immunology  
 University Medical Center Mainz  
 Obere Zahlbacherstraße 63, 55131 Mainz, Germany  
 D. Schuppan  
 Division of Gastroenterology, Beth Israel Deaconess Medical Center  
 Harvard Medical School Boston  
 330 Brookline Ave, Boston, MA 02215, USA  
 H. Schild  
 Institute for Immunology  
 University Medical Center Mainz  
 Langenbeckstraße 1, 55131 Mainz, Germany  
 B. Biersack  
 Organic Chemistry Laboratory  
 University of Bayreuth  
 Universitätsstraße 30, 95447 Bayreuth, Germany

 The ORCID identification number(s) for the author(s) of this article can be found under <https://doi.org/10.1002/marc.202200095>

© 2022 The Authors. Macromolecular Rapid Communications published by Wiley-VCH GmbH. This is an open access article under the terms of the Creative Commons Attribution-NonCommercial License, which permits use, distribution and reproduction in any medium, provided the original work is properly cited and is not used for commercial purposes.

DOI: 10.1002/marc.202200095

(TLR7/8), or CpG-oligonucleotides (TLR9).<sup>[8,9]</sup> These receptors are residing, for instance, on dendritic cells that orchestrate efficient immune responses through antigen presentation.<sup>[10,11]</sup> TLR agonists are therefore suitable adjuvants for vaccination purposes (e.g., the TLR7/8 imidazoquinoline agonist IMDG is currently successfully applied by Bharat Biotech in their Covid-19 vaccine Covaxin (BBV152)).<sup>[12–14]</sup> Additionally, academia-driven research has confirmed the applicability of TLR stimulation for the treatment of cancer.<sup>[15,16]</sup> By administering TLR agonists via nano-sized drug carriers, they can more precisely be maneuvered to lymph nodes, the tumor microenvironment, or other sites of the immune system and thereby dampen undesired off-target effects.<sup>[17,18]</sup> The hydrophobic TLR7/8 agonist 2-propylthiazolo[4,5-c]quinolin-4-amine (CL075)<sup>[19,20]</sup> is highly attractive for such purposes. It provides only low aqueous solubility, but nano-sized micellar carriers have been demonstrated to encapsulate CL075 or similar TLR7/8 agonists into their hydrophobic cores.<sup>[21–23]</sup>

Among different types of polymeric materials for micellar drug delivery, aliphatic carbonates have lately been discussed as attractive alternatives.<sup>[24]</sup> Due to their hydrolytic biodegradability and biocompatibility, these features strongly suggest their translatability into clinical applications.<sup>[25–27]</sup> The carbonate motif has already been employed for degradable systems carrying carbonate moieties in the side chain<sup>[28,29]</sup> and, more significantly, as backbone in aliphatic polycarbonates.<sup>[30–32]</sup> Using amphiphilic polycarbonate block copolymers, nanoparticulate systems can be self-assembled and applied for various therapeutic applications.<sup>[33–35]</sup> However, these materials often lack the possibility to covalently introduce additional functionalities, such as dyes for precise carrier monitoring during delivery.

We herein present an elegant way to design such materials by employing the active ester chemistry for controlled polymer end group functionalization.<sup>[36]</sup> This approach requires the synthesis of polymers with highly defined end groups followed by a quantitative activation and conjugation of the cargo, as lately demonstrated by us for RAFT polymerization-derived end groups.<sup>[37]</sup> In the current study, we apply this approach for the first time to polycarbonate-based block copolymers obtained by organocatalytic ring-opening polymerization. The primary hydroxy end group could be converted into a pentafluorophenyl carbonate and subsequently derivatized with primary amine bearing fluorescent dyes. This enabled us to efficiently track micelles derived from these block copolymers in the blood stream and during cell uptake. We additionally quantified efficient drug encapsulation, including the TLR7/8 thiazoloquinoline agonist CL075, which confirmed its immune stimulatory potential on various types of primary dendritic cells. Altogether, these features promote the applicability of end group dye-labeled polycarbonate block copolymers for micellar (immuno-)drug delivery.

## 2. Results and Discussion

To provide access to such highly defined polymeric carrier systems, it is crucial to control block copolymer length and

assure desired end groups. Especially for ring-opening polymerization reactions, it is necessary to use highly pure starting materials. The herein presented polycarbonate-based micelles were self-assembled from end group functionalized mPEG<sub>113</sub>-*b*-poly(MTC-OBn)<sub>15</sub> block copolymers. For a well-defined synthesis of these polymers, the highly pure 5-methyl-5-benzyloxycarbonyl-1,3-dioxan-2-one (MTC-OBn) monomer<sup>[38]</sup> was used (as shown by X-ray diffraction of the recrystallized monomers, **Figure 1A** and characterization data in Figures S1–S3, Supporting Information). All starting materials had to be dried by azeotropic distillation with benzene prior to polymerization under inert atmosphere. During polymerization, side reactions such as backbiting and homopolymerization had to be avoided to yield end group defined polymers. Therefore, ring-opening polymerizations were conducted at decreased temperatures of –20 °C using the organocatalyst 1,8-diazabicyclo[5.4.0]undec-7-ene (DBU). Polymerization conditions were first tested by homopolymerization of MTC-OBn, and detailed product analyses including MALDI-ToF mass spectrometry confirmed the integrity of end group defined homopolymers (compare **Figure S4**, Supporting Information).

The optimized reaction conditions were then successfully applied for block copolymerization, initiated from a mPEG<sub>113</sub>-OH macroinitiator. After precipitation in diethyl ether, block copolymers with an increase of molecular weight compared to mPEG<sub>113</sub> and narrow dispersities of 1.05 were yielded (**Figure 1B**). Further analyses such as DOSY-NMR (**Figure 1C**) and MALDI-ToF mass spectrometry demonstrated again the high definition of the mPEG<sub>113</sub>-*b*-poly(MTC-OBn)<sub>15</sub> block copolymer product (**Figures S5** and **S9**, Supporting Information).

Prior to block copolymer self-assembly into micelles, we aimed to label the carrier material with a fluorescent dye to track the material in a biological system. For circulation in the blood stream we selected the fluorescent dye Alexa Fluor 647 (AF647), while for cellular uptake experiments we chose tetramethyl rhodamine (TMR). For covalent conjugation to the mPEG<sub>113</sub>-*b*-poly(MTC-OBn)<sub>15</sub> block copolymers, the primary hydroxy end groups were activated by reaction with bis(pentafluorophenyl)carbonate to form a highly reactive pentafluorophenyl carbonate (**2**) (**Figure 2A**). This reaction sequence allows the defined synthesis of single labeled polymers with almost unaltered molecular integrity, as verified by size exclusion chromatography (SEC; **Figure 2B**, full spectra **Figure S8**, Supporting Information). Successful labeling was further demonstrated by SEC using UV–vis detection at dye specific wavelengths. Compared to the non-labeled starting material, both AF647- and TMR-labeled block polymers provided absorptions at the respective wavelengths 647 (for AF647) and 549 nm (for TMR) (**Figure 2B**), which was also proven by recording the whole UV–vis spectra of the purified polymers (**Figure 2C**). Moreover, MALDI-ToF mass spectrometry and NMR spectroscopy further confirmed the high specificity of the active ester approach and the covalent conjugation of one single dye molecule to the block copolymer (compare **Figures S6–S9**, Supporting Information).

For the preparation of drug-loaded polymeric micelles, we next opted for the solvent-evaporation method due to its high encapsulation efficiency and high reproducibility.<sup>[39]</sup> Non-encapsulated drug outside of the micellar core usually precipitates during this process and can easily be filtered off by standard sterile filtration

L. Nuhn  
Chair of Macromolecular Chemistry, Faculty of Chemistry and Pharmacy  
Julius Maximilian University Würzburg  
Röntgenring 11, 97070 Würzburg, Germany

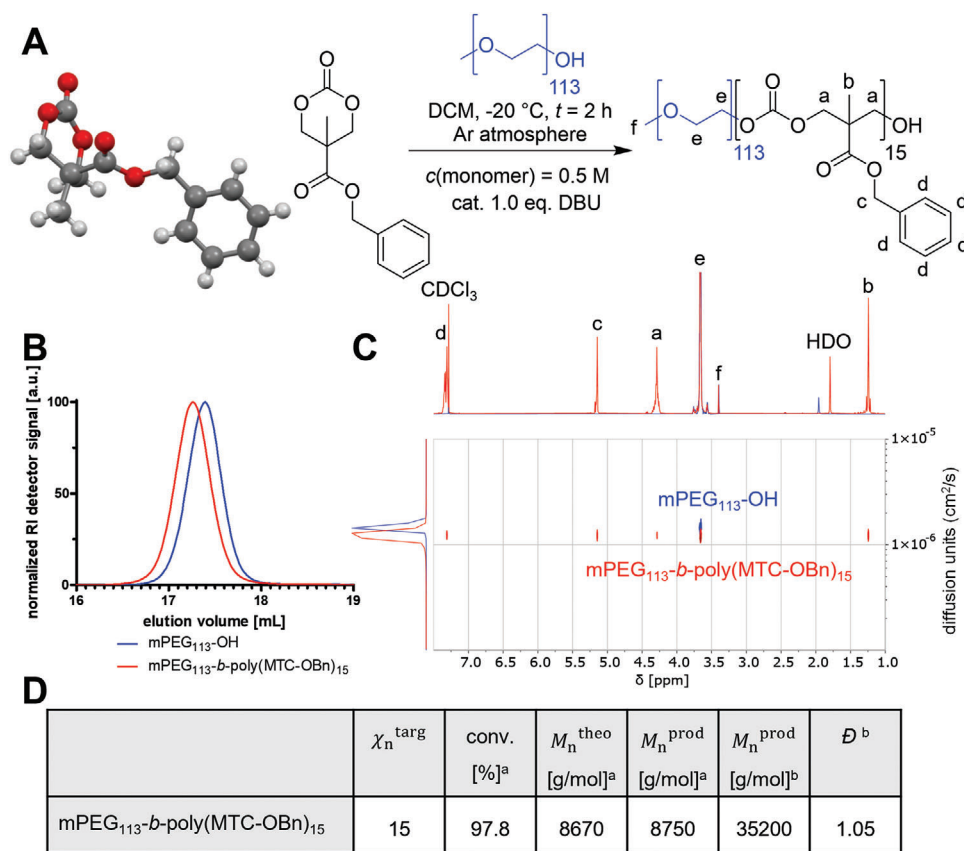


**Figure 1.** Synthesis and characterization of polycarbonate block copolymer functionalized mPEG<sub>113</sub>-b-poly(MTC-OBn)<sub>15</sub>. A) Crystal structure of 6-ring carbonate monomer 5-methyl-5-benzoyloxycarbonyl-1,3-dioxan-2-one (MTC-OBn) and ring-opening polymerization of MTC-OBn initiated from mPEG<sub>113</sub> using the organocatalyst 1,8-diazabicyclo[5.4.0]undec-7-ene (DBU). B) Size exclusion chromatogram<sup>b</sup> (SEC, refractive index, RI) of mPEG<sub>113</sub>-b-poly(MTC-OBn)<sub>15</sub> block copolymer compared to the mPEG<sub>113</sub> macroinitiator. Block copolymers show a shift toward higher molecular weight (lower elution volume) but a similar narrow distribution ( $\mathcal{D} = 1.05$ ). C) <sup>1</sup>H DOSY-NMR of block copolymers (red) provide a higher diffusion coefficient and additional signals for the polycarbonate block compared to mPEG<sub>113</sub> (blue). D) Characterization summary of mPEG<sub>113</sub>-b-poly(MTC-OBn)<sub>15</sub>. [<sup>a</sup>Determined by <sup>1</sup>H NMR analysis. <sup>b</sup>Determined by HFIP (hexafluoroisopropanol) size exclusion chromatography, calibrated with PMMA standards.]

processes. The feasibility of this approach was first demonstrated by encapsulating the hydrophobic compound 3,3'-((3,4-difluorophenyl)methylene)bis(1*H*-indole) (DIM-DF, **Figure 3A**). The anticancer drug DIM-DF was chosen as a model drug<sup>[40]</sup> due to its high  $\log(P)$  value of 4.5 and its straightforward quantification by <sup>19</sup>F NMR. Formulations of DIM-DF were prepared by dropping a polymer–drug mixture in acetone of 10:1 polymer to drug (weight-to-weight ratio, 9.09 wt% drug) into water. During the evaporation of the volatile acetone, micelles were formed by spontaneous self-assembly. Simultaneously the hydrophobic drug molecule is encapsulated inside the core. Polymeric micelles with uniform monomodal sizes were yielded and characterized by dynamic light scattering (DLS; **Figure 3D**, z-average hydrodynamic diameter of 26.0 nm, PDI = 0.09). We assume that the strong  $\pi$ - $\pi$  interaction of the benzyl ester side chains inside the micelle favor the encapsulation of hydrophobic compounds that are rich in aromatic groups, too.<sup>[41,42]</sup> This feature might also stabilize the block copolymer micelles when adsorbed and dried on flat surfaces, as atomic force microscopy (AFM) images still confirmed the presence of spherical-shaped nanoparticles (compare **Figure S10**, Supporting Information). Interestingly, precise quantification of the drug load was achieved by analyzing freeze-

dried material by <sup>19</sup>F NMR spectroscopy and comparing the value to a DIM-DF standard calibration (**Figure 3B**). Via this method a drug load of 8.97 wt% was determined. Compared to the targeted drug load of 9.09 wt%, this solvent-evaporation process yielded a high encapsulation efficiency of 98.6% (**Figure 3E** and **Figure S12**, Supporting Information for calculations as well as additional UV–vis spectra in **Figure S11**, Supporting Information).

While for biological testing of DIM-DF-loaded micelles the AF647-labeled block copolymers were used, the encapsulation of the hydrophobic immunodrug CL075 could in analogy be performed using the TMR-labeled block copolymers. Due to the partial solubility of CL075 at the slightly acidic pH, which occurs in Millipore water, the CL075-loaded micelles were prepared in PBS at pH 7.4. Similar to the preparation of DIM-DF-loaded micelles, we checked for a precise quantification method for CL075 encapsulation after micelle formulation. Interestingly, CL075 provides a typical absorbance at 350 nm, which could be compared to a calibration of the drug itself (**Figure 3C**). This afforded a drug load of 1.78 wt% (at an aimed drug load 1.96 wt%) and confirmed again the high encapsulation efficiency of 90.6% for this formulation method (**Figure 3E** and **Figure S13**, Supporting Information for calculations).

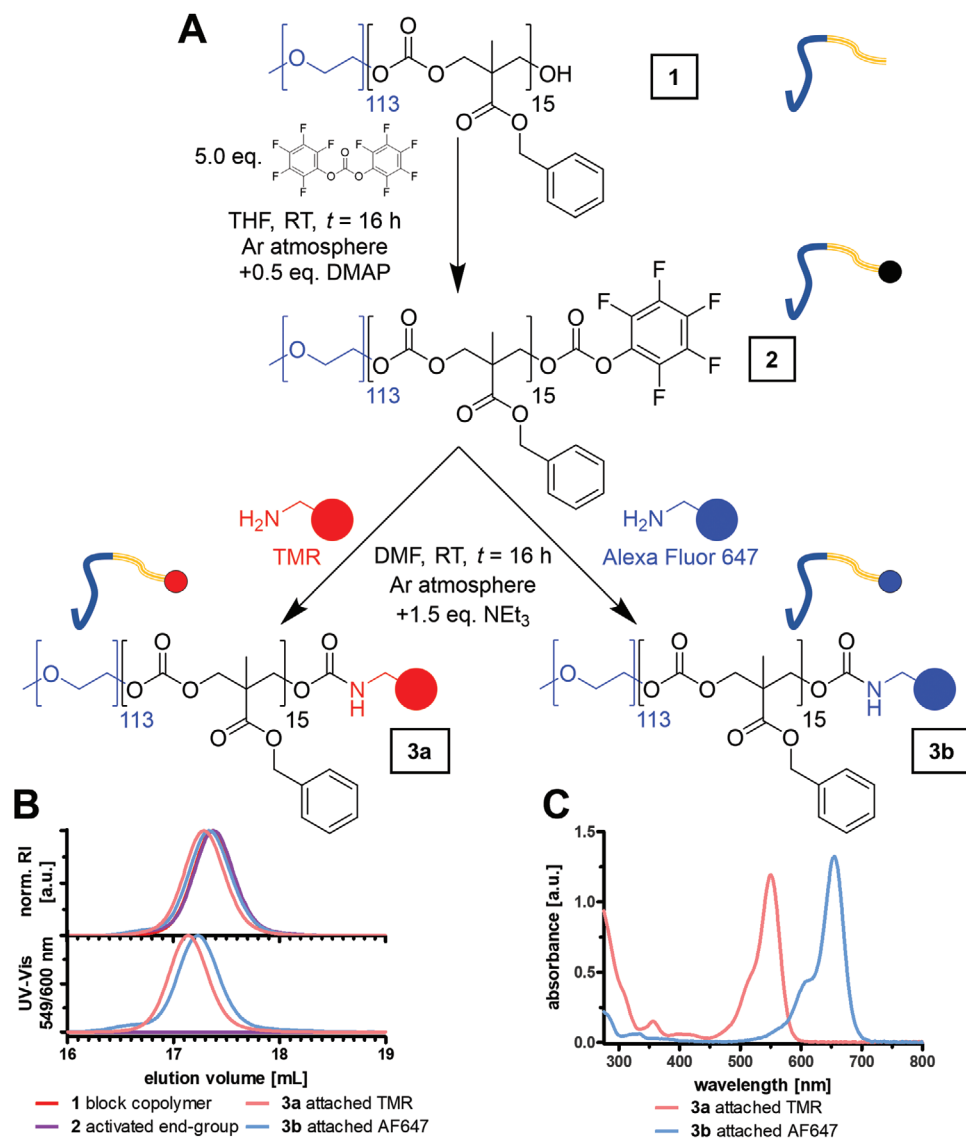


**Figure 2.** Synthesis of end group functionalized polycarbonate block copolymers. A) Through reactive ester carbonate activation the block copolymer 2 is subsequently aminolyzed with primary amine functionalized dye molecules yielding block copolymer 3a (with tetramethyl rhodamine [TMR]) and 3b (with Alexa Fluor 647 [AF647]). B) HPLC SEC elugram of the respective block copolymers showing highly defined end group functionalized block copolymers, both by normalized (norm.) RI traces (top) and additional absorption traces at dye specific wavelengths (bottom, UV traces at 549 nm for TMR detection and 600 nm for AF647). C) Corresponding UV–vis absorbance spectra of the block copolymers 3a and 3b.

With these drug-loaded micelles, formulated from well-defined dye-labeled block copolymers, their performance was tested in a biological context. Aiming for the application as an anticancer drug carrier with prolonged blood circulation to accumulate in tumorous tissue (e.g., via the enhanced permeability and retention (EPR) effect<sup>[43]</sup>), it was initially investigated if the particles remain stable under physiologically relevant protein-rich conditions. Therefore, particles were incubated with human blood serum for 1 h at 37 °C followed by a multi-angle DLS analysis established by Rausch et al. (Figure 4A).<sup>[44]</sup> For mPEG<sub>113</sub>-b-poly(MTC-OBn)<sub>15</sub> micelles no significant differences were found between recorded and predicted autocorrelation curves at multiple angles indicating that the micelles do not aggregate upon protein incubation but remain stable. Identical results were ob-

tained for the DIM-DF drug-loaded micelles, too (see Figure S14, Supporting Information).

Encouraged by these promising results, the circulation of the micelles in the blood stream of zebrafish embryos was recorded. The AF647-labeled polymeric micelles provide ideal fluorescent properties to track them within the blood vessels of the transparent zebrafish embryos (Figure 4B1). Fortunately, polymeric micelles were found circulating in the zebrafish embryos over 72 h after injection in the posterior cardinal vein (Figure 4B2). After an initial drop, about 50% of the injected particles were found in the blood stream after 4 h and around 30% after 24 h. Interestingly, this amount remained stable for the following 2 days. After 72 h, still ≈30% of both DIM-DF-loaded and empty micelles were found circulating

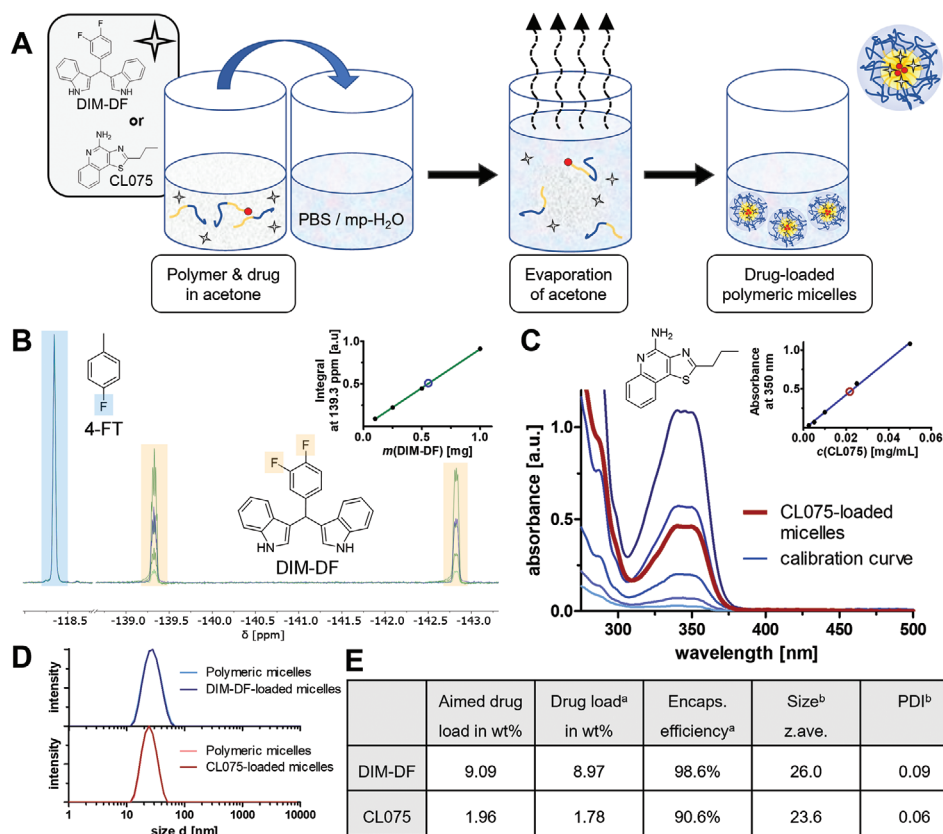


**Figure 3.** Fabrication and characterization of drug-loaded polymeric micelles prepared by solvent-evaporation of end group functionalized polycarbonate block copolymers. A) Self-assembly process of micelles by solvent evaporation. The polymer/drug solution is dropped into aqueous media at a volumetric 1:1 ratio of acetone and water. During evaporation of the volatile acetone, the drug-loaded micelles are formed. Micelles were either loaded with DIM-DF, a hydrophobic anticancer drug, or the immunostimulatory TLR7/8 agonist CL075. B) Determination of DIM-DF drug load by  $^{19}\text{F}$ -NMR using a DIM-DF calibration curve ( $y = 0.9108 \text{ mg}^{-1} \cdot x - 0.0027$ ). Solvent was spiked with 4-fluorotoluene as reference compound for spectrum intensity normalization. Freeze-dried DIM-DF-loaded micelles (dissolved in  $\text{DMSO-}d_6$ ) were measured to calculate the drug load. C) Determination of CL075 drug load by a UV-vis calibration curve ( $y = 22.445 \text{ mL} \cdot \text{mg}^{-1} \cdot x - 0.0276$ ). All measurements were recorded in a volumetric 1:1:2 mixture of water:PBS:THF. Drug-loaded micelles were diluted similarly using a water/THF mixture and measured. D) Particle sizes recorded by DLS showing narrow monomodal distributions of both DIM-DF-loaded micelles (top) and CL075-loaded micelles (bottom). E) Characterization summary of DIM-DF and CL075-loaded end group functionalized polycarbonate block copolymer micelles. [<sup>a</sup>Determined by  $^{19}\text{F}$  NMR (DIM-DF)/UV-vis (CL075). <sup>b</sup>Determined by DLS.]

in the blood stream and, thus, provide similar circulation properties as reported for other effective long-circulating particles.<sup>[45–48]</sup>

Beyond micelles' stability, we were also interested in their potential hydrolytic degradability rendered by the polycarbonate backbone. For that purpose, particle samples were measured by DLS at different time points. In PBS, the micelles remained stable even after several months (Figure S15, Supporting Information) supporting their favorable long shelf life. Alkaline conditions, however, immediately triggered their gradual disintegration (Figure 4C1). Upon addition of 10 vol% 1 M NaOH (pH 13), particles rearranged and immediately formed large aggregates with sizes larger than 100 nm. We followed this aggregation process and observed a slow disintegration over a time span of  $\approx 2$  days with decreasing particle sizes and drastically declining particle count rates (Figure 4C1). Finally, complete degradation occurred with sizes below 5 nm. At lower pH conditions (pH 9.2) a slower degradation was observed (Figures S15 and S16, Supporting Information—degradation half-life  $t_{1/2} = 17.8$  h at pH 9.2 compared to  $t_{1/2} = 9.3$  h at pH 13).

Mass spectrometric analysis (Figure 4C2) of the degradation products could be performed with the TMR-labeled block copolymers after incubation in ammonium bicarbonate buffer (10  $\mu\text{M}$ , pH 8, see Figure S17, Supporting Information for full ESI-MS spectrum). Interestingly, besides multiple charged species of the remaining mPEG<sub>113</sub>-OH macroinitiator, the expected degradation product of the TMR end group could be found as carbamate motif attached to one single repeating unit of decarboxylated monomer MTC-OBn ( $M = 764.34 \text{ g mol}^{-1}$ , recorded as  $m/z = 765.34 [M + H]^+$ ). The appearance of this degradation product once again proves the successful attachment of the dye and, most notably, the degradability of poly(MTC-OBn) through the polycarbonate motif. Interestingly, under the applied conditions hydrolysis did not occur at the benzyl ester side chain, but at the more labile carbonate groups.<sup>[49]</sup> These degradation experiments exemplify the general hydrolytic degradation potential of polycarbonates (under base catalyzed conditions, potentially also mediated by degrading enzymes, as reported earlier for polycarbonate bulk materials).<sup>[24,50]</sup> However, they also disclose their limited relevance at physiological pH

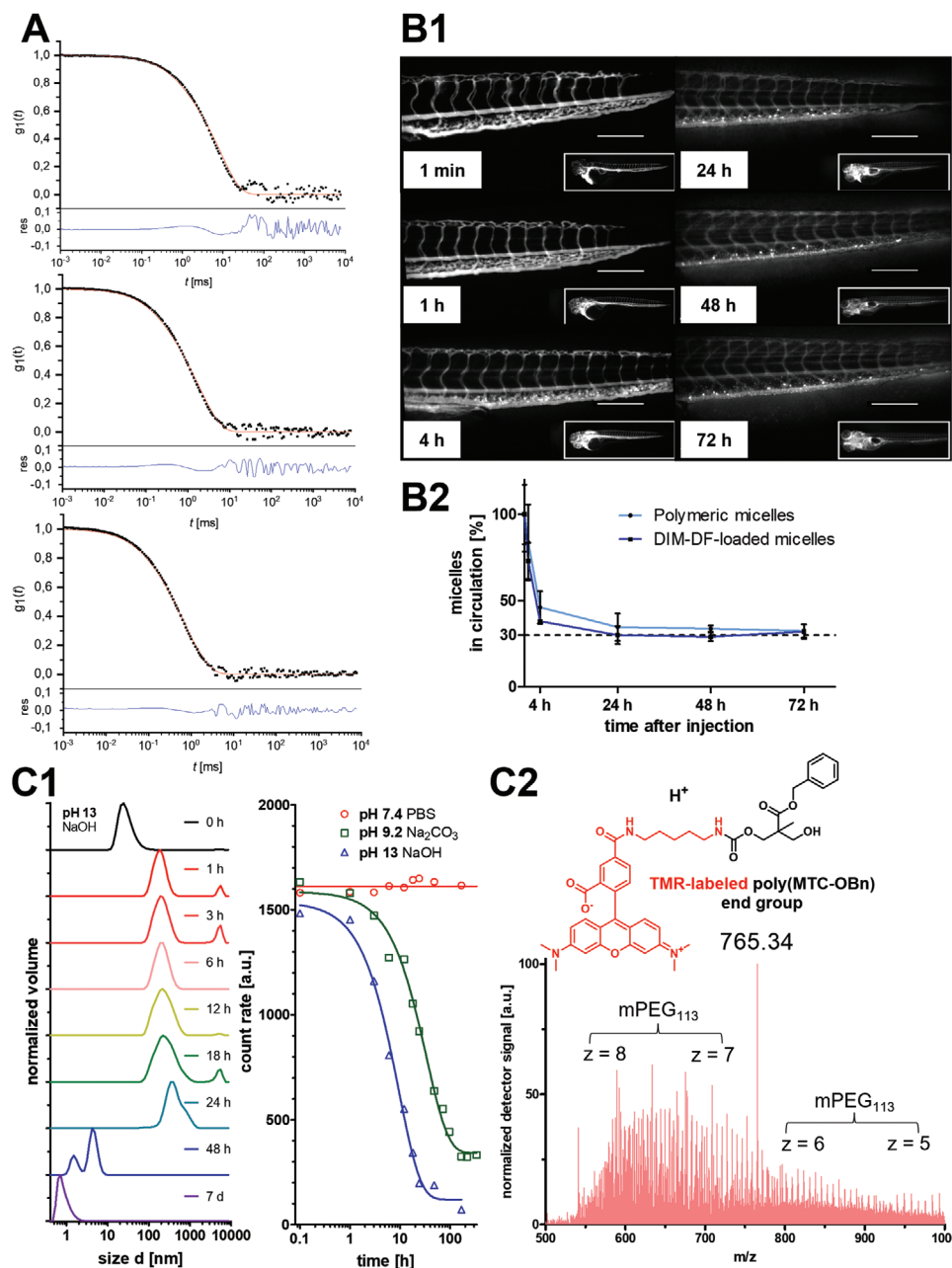


**Figure 4.** Evaluation of dye end group functionalized polycarbonate block copolymer micelles in biological media and their hydrolytic degradation potential. A) Blood plasma incubation studies by multi-angle DLS of mPEG<sub>113</sub>-b-poly(MTC-OBn)<sub>15</sub> micelles. After incubation for 1 h in human blood plasma, their autocorrelation curves were recorded at different angles (30°, 60°, and 90°, from top to bottom—black dots) and compared to the sum of autocorrelation curves obtained from individual measurements of plasma and micelles (red curve). B) Blood circulation of AF647-labeled micelles in zebrafish embryos investigated by fluorescence intensity at multiple time points over 72 h (B1). Even after 72 h, ≈30% of the micelles could still be found circulating in the blood stream (B2). C) Hydrolytic degradation behavior of polycarbonate micelles. C1) Micelles fully disintegrated after addition of 10 vol% 1 M NaOH, as indicated by DLS analysis of size changes (first aggregation to larger particles, followed by total disintegration—left) and declining particle count rates within the first 48 h (right, blue curve). Incubation at pH 9.2 (green curve) triggers analogous degradation within ≈4 days. At pH 7.4 in PBS (red line) particles count rates as well as sizes remain stable (compare also Figures S15 and S16, Supporting Information). C2) Mass spectrometric analysis of the degradation products from hydrolyzed TMR-labeled polymeric micelles (note that an incubation with ammonium bicarbonate buffer [10 μM, pH 8] was necessary for ESI-MS in the presence of volatile salts). Interestingly, besides multiple charged species of the remaining mPEG-OH macroinitiator (z = 5, 6, 7, and 8), the TMR-labeled end group was also found as carbamate attached to the decarboxylated MTC-OBn monomer.

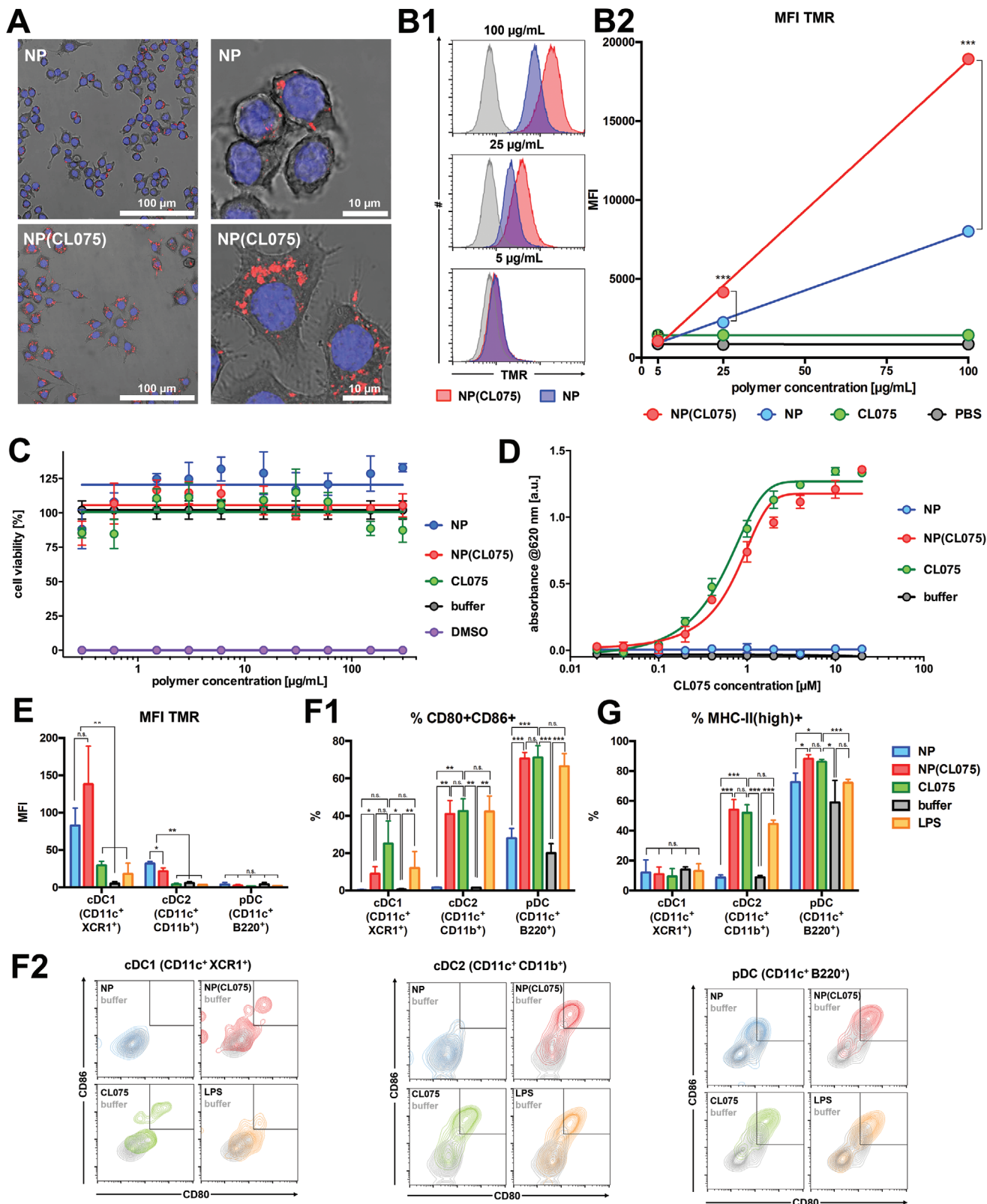


**Figure 5.** Biological evaluation of TMR end-group-labeled block copolymer micelles loaded with the immune stimulatory TLR7/8 agonist CL075. A) Confocal microscopy of RAW Blue macrophages incubated with  $100 \mu\text{g mL}^{-1}$  empty (NP) and CL075-loaded NP(CL075) micelles derived from TMR end-group-labeled polycarbonate block copolymers (red: polymer—blue: nuclei stained with DAPI). B) Flow cytometry of RAW Blue macrophages incubated with increasing doses of empty (NP) and CL075-loaded NP(CL075) micelles determined by B1) histogram and B2) mean fluorescence intensity (MFI)

values at which mPEG<sub>113</sub>-*b*-poly(MTC-OBn)<sub>15</sub> so far did not hydrolyze. Possibly, water exclusion within the hydrophobic polycarbonate core enhances hydrolytic stability, thereby requiring increased pH values (or degrading enzymes) for facilitating biodegradation.

The CL075 immunodrug-loaded block copolymer micelles were finally checked for their pharmacologic activity. TMR-labeled micelles were used and first checked in vitro for their cellular uptake behavior on RAW macrophages. For that purpose, cells were incubated overnight with and without CL075-loaded micelles and then analyzed by confocal microscopy (Figure 5A and Figures S20–S22, Supporting Information). Compared to empty micelles (NP), the drug-loaded micelles (NP(CL075)) revealed a much stronger internalization and accumulation in intracellular vesicular compartments. They also affected cell morphology (Figure 5A) which correlated with the TLR7/8 receptor stimulation of the CL075 payload (compare Figures S20–S22, Supporting Information).

This cell uptake was further quantified by flow cytometry (Figure 5B and Figure S19, Supporting Information). A linear dose dependency of particle internalization was found, and the significantly enhanced uptake of NP(CL075) was confirmed (Figure 5B). Interestingly, no influence on cell viability was observed over a broad range of polymer concentrations up to 300 µg mL<sup>-1</sup> (Figure 5C—note also that CL075 drug loading or the free drug itself did not affect the cell viability at the applied dose regime).

The Raw macrophages used for these experiments are genetically modified to provide a reporter function upon TLR7/8 receptor stimulation (RAW Blue macrophages). Upon subsequent activation of their NF-κB pathway, these cells secrete alkaline phosphatase, which can easily be quantified spectrophotometrically from the cell culture supernatant by a Quanti Blue assay. A broad range of TLR7/8 agonist CL075 concentrations formulated in the block copolymer micelles was screened and compared to empty micelles (Figure 5D). While the empty micelles NP did not affect the TLR stimulation, a sub-µM activation was found for drug-loaded micelles NP(CL075), which was identical to the drug alone applied from a DMSO stock solution. Note that if the drug was diluted in PBS from an aqueous stock solution (prepared by the solvent-evaporation process without block copolymers), its activity was tenfold lower (Figure S18, Supporting Information). Considering the limited applicability of DMSO formulation for in vivo purposes (according to the toxicity of DMSO demonstrated in Figure 5C), the end group functionalized polycarbonate block copolymer micelles provide ideal features for encapsulation and release of CL075. Micellar delivery may further improve the biodistribution during in vivo applications and focus its delivery ideally to draining lymph nodes or other lymphoid organs, as demonstrated for other TLR7/8 agonist nanoparticle formulations by us and others before.<sup>[6,18,51–54]</sup>

Finally, to evaluate the immune stimulation potency of the CL075-loaded micelles, we investigated their effect on dendritic

cells (DC) derived from murine bone marrow (BMDC). Generally, DC are considered as the most effective antigen-presenting cells and therefore are of major importance to get stimulated for vaccination or cancer immunotherapy purposes. Upon cultivation for 1 week in Fms-related tyrosine kinase 3 receptor (FLT3) ligand supplemented media, bone marrow cells differentiate into different subtypes of DC characterized by their specific surface markers (compare Figure S23, Supporting Information). Among them, conventional (myeloid) DC type 1, cDC1, is identified as CD11c<sup>+</sup> XCR1<sup>+</sup> and considered to preferentially trigger prime type 1 immune responses (cytotoxic T cell responses against viral infections or cancer).<sup>[11]</sup> Additionally, conventional (myeloid) DC type 2, cDC2, provides a CD11c<sup>+</sup> CD11b<sup>+</sup> surface expression and is known to induce type 2 immune responses (against parasites or bacteria),<sup>[55]</sup> while plasmacytoid dendritic cells, pDC, identified as CD11c<sup>+</sup> B220<sup>+</sup>, are renowned for their high type 1 interferon secretion and pronounced antigen-presentation capacity.<sup>[56,57]</sup>

After incubation of FLT3 ligand differentiated BMDCs for 24 h with empty and CL075-loaded micelles (and soluble CL075 and the TLR4 agonist LPS as control, both from a DMSO stock solution), we characterized micelle uptake by the DC subpopulations and their activation marker expression profile using flow cytometry. TMR fluorescence detection served to quantify micelle uptake into the three different DC subpopulations. Interestingly, the highest micelle uptake was observed for cDC1, followed by cDC2, but scarcely any uptake in pDC (Figure 5E and Figure S24, Supporting Information). Micelle uptake in cDC1 is desired in order to initiate cytotoxic T cell responses that are most favorable for cancer immunotherapy. A slightly higher (but not significant) uptake was found for the CL075-loaded NP(CL075) compared to empty micelles NP in cDC1, while for cDC2 the empty micelles seemed to get internalized more effectively (Figure 5E and Figure S24, Supporting information).

We also analyzed the maturation state for all three DC subtypes by quantifying the surface expression of the co-stimulatory molecules CD80 and CD86 as markers for dendritic cell maturation for antigen presentation (Figure 5F1, F2 and Figure S25, Supporting Information). For all three DC subpopulations (cDC1, cDC2, and pDC), the drug-loaded micelles NP(CL075) induced significantly upregulated expression of both co-stimulatory maturation markers CD80 and CD86, while the empty micelles NP remained immunologically silent (like the buffer control). Similar maturation levels could be obtained for the two positive controls, CL075 and LPS, demonstrating the safe delivery and efficient CL075 release from the end group block copolymer micelles.

Finally, we also checked for the surface expression of the antigen-presenting major histocompatibility class II (MHCII complex) in all three DC subtypes (Figure 5G and Figure S23, bottom, Supporting Information). While the expression and stimulation were—as expected—rather low in cDC1 (they rather favor

analyses ( $n = 3$ ,  $***p < 0.001$ ). C) Cell viability determined by MTT assay ( $n = 4$ ). D) TLR7/8 receptor stimulation by Raw Blue assay ( $n = 4$ ). E) Cell uptake into FLT3 ligand differentiated BMDC subpopulations analyzed by flow cytometry ( $n = 4$ ,  $*p < 0.05$ ,  $**p < 0.01$ ,  $***p < 0.005$ ). F) CD80 and CD86 expression of FLT3 ligand differentiated BMDC subpopulations analyzed by F1) flow cytometry and F2) their corresponding histograms ( $n = 4$ ,  $*p < 0.05$ ,  $**p < 0.01$ ,  $***p < 0.001$ ). G) MHCII-high expression of FLT3 ligand-derived BMDC subpopulations analyzed by flow cytometry ( $n = 4$ ,  $*p < 0.05$ ,  $**p < 0.01$ ,  $***p < 0.001$ ).



antigen presentation via MHC I), a significant increase of cells that highly express MHC II was observed in cDC2 after incubation with NP(CL075), similar to a stimulation with CL075 alone or LPS. Consequently, micelle-guided CL075 delivery can in principle also boost type 2 immune responses. For pDCs that already provide quite a high MHC II expression profile, NP(CL075) could also enhance their expression a bit further and, thus, may also enhance type 1 immune responses. Altogether, these findings underline that our TLR7/8 agonist-loaded micelles confer a safe and effective maturation and antigen-presentation capacity for various types of DC which are capable of eliciting a broad spectrum of type I and type II immune responses. These observations make our micelles highly attractive for instance as adjuvants during vaccination or cancer immunotherapy.

### 3. Conclusion

We could demonstrate the successful synthesis and application of single dye end group modified polycarbonate block copolymers and their resulting (immuno-)drug-loaded micelles. Highly controlled ring-opening polymerizations yielded alcohol end-group-defined block copolymers that could be activated as reactive pentafluorophenyl ester carbonates. To the best of our knowledge, the approach of installing single reactive end groups onto aliphatic polycarbonates has not been reported before. It allows us to access single dye-labeled polymer chains by aminolysis with various primary amine functionalized dyes. Via a subsequent solvent-evaporation method, these end group dye-labeled block copolymers could reproducibly be self-assembled into defined polymeric micelles of sizes around  $\approx 25$  nm and narrow PDI below 0.1. By including hydrophobic drugs during the self-assembly process, micellar formulations with high drug loads of 8.87 wt% for the anticancer drug DIM-DF and 1.74 wt% for the immunodrug CL075 were achieved with high encapsulation efficiencies above 87%. These micelles were shown to not only solubilize the cargo but to nicely envelop the drug, avoid protein aggregation in human blood plasma and promote prolonged circulation in the blood stream of zebrafish embryos. Hydrolytic disintegration of the micelles was only possible under alkaline conditions revealing expected end group degradation products. Biological evaluation of the immune-drug CL075-loaded micelles demonstrated uptake into key antigen-presenting cells as well as sufficient TLR7/8 activation both in an in vitro reporter cell line and in different subpopulations of bone marrow delivered primary dendritic cells. Overall, these experiments demonstrate that end group modified polycarbonate block copolymers seem highly suitable for the tracking of the encapsulation and delivery of various hydrophobic (immuno-)drugs and, thus, for paving the way of these drugs toward vaccination or cancer (immuno-)therapy.

### Supporting Information

Supporting Information is available from the Wiley Online Library or from the author.

### Acknowledgements

This work was gratefully supported by the DFG through the Emmy Noether program (to L.N.) and the CRC/SFB 1066 (to L.N., S.G., M.B., H.S., and

D.S.). Dieter Schollmeyer is acknowledged for X-Ray Diffraction Analysis, Jutta Schnee and Stephan Türk for MALDI-ToF measurements, Christine Rosenauer for multi-angle DLS measurements, and Manfred Wagner for NMR measurements.

Open access funding enabled and organized by Projekt DEAL.

### Conflict of Interest

The authors declare no conflict of interest.

### Data Availability Statement

The data that support the findings of this study are available in the supplementary material of this article.

### Keywords

aliphatic polycarbonates, block copolymers, immunodrug delivery, micelles, self-assembly

Received: February 2, 2022  
Published online: April 10, 2022

- [1] M. Talelli, M. Barz, C. J. F. Rijcken, F. Kiessling, W. E. Hennink, T. Lammers, *Nano Today* **2015**, *10*, 93.
- [2] R. Duncan, R. Gaspar, *Mol. Pharmaceutics* **2011**, *8*, 2101.
- [3] Z. Ahmad, A. Shah, M. Siddiq, H.-B. Kraatz, *RSC Adv.* **2014**, *4*, 17028.
- [4] H. Cabral, K. Kataoka, *J. Controlled Release* **2014**, *190*, 465.
- [5] Y. Mai, A. Eisenberg, *Chem. Soc. Rev.* **2012**, *41*, 5969.
- [6] L. Nuhn, N. Vanparijs, A. De Beuckelaer, L. Lybaert, G. Verstraete, K. Deswarte, S. Lienenklaus, N. M. Shukla, A. C. D. Salyer, B. N. Lambrecht, J. Grooten, S. A. David, S. De Koker, B. G. De Geest, *Proc. Natl. Acad. Sci. U. S. A.* **2016**, *113*, 8098.
- [7] J. Shi, P. W. Kantoff, R. Wooster, O. C. Farokhzad, *Nat. Rev. Cancer* **2017**, *17*, 20.
- [8] M. Saeed, J. Gao, Y. Shi, T. Lammers, H. Yu, *Theranostics* **2019**, *9*, 7981.
- [9] S. Kaczanowska, A. M. Joseph, E. Davila, *J. Leukoc. Biol.* **2013**, *93*, 847.
- [10] K. Palucka, J. Banchereau, *Nat. Rev. Cancer* **2012**, *12*, 265.
- [11] M. Merad, P. Sathe, J. Helft, J. Miller, A. Mortha, *Annu. Rev. Immunol.* **2013**, *31*, 563.
- [12] R. Ella, K. M. Vadrevu, H. Jogdand, S. Prasad, S. Reddy, V. Sarangi, B. Ganneru, G. Sapkal, P. Yadav, P. Abraham, S. Panda, N. Gupta, P. Reddy, S. Verma, S. Kumar Rai, C. Singh, S. V. Redkar, C. S. Gillurkar, J. S. Kushwaha, S. Mohapatra, V. Rao, R. Guleria, K. Ella, B. Bhargava, *Lancet Infect. Dis.* **2021**, *21*, 637.
- [13] R. Ella, S. Reddy, H. Jogdand, V. Sarangi, B. Ganneru, S. Prasad, D. Das, D. Raju, U. Praturi, G. Sapkal, P. Yadav, P. Reddy, S. Verma, C. Singh, S. V. Redkar, C. S. Gillurkar, J. S. Kushwaha, S. Mohapatra, A. Bhate, S. Rai, S. Panda, P. Abraham, N. Gupta, K. Ella, B. Bhargava, K. M. Vadrevu, *Lancet Infect. Dis.* **2021**, *21*, 950.
- [14] R. Ella, S. Reddy, W. Blackwelder, V. Potdar, P. Yadav, V. Sarangi, V. K. Aileni, S. Kanungo, S. Rai, P. Reddy, S. Verma, C. Singh, S. Redkar, S. Mohapatra, A. Pandey, P. Ranganadin, R. Gumashta, M. Multani, S. Mohammad, P. Bhatt, L. Kumari, G. Sapkal, N. Gupta, P. Abraham, S. Panda, S. Prasad, B. Bhargava, K. Ella, K. M. Vadrevu, P. Aggarwal, et al., *Lancet* **2021**, *398*, 2173.
- [15] Y. Mi, C. T. Hagan, B. G. Vincent, A. Z. Wang, *Adv. Sci.* **2019**, *6*, 1801847.

- [16] J. Stickdorn, L. Stein, D. Arnold-Schild, J. Hahlbrock, C. Medina-Montano, J. Bartneck, T. Ziss, E. Montermann, C. Kappel, D. Hobernik, M. Haist, H. Yurugi, M. Raabe, A. Best, K. Rajalingam, M. Radsak, S. David, K. Koynov, M. Bros, S. Grabbe, H. Schild, L. Nuhn, *ACS Nano* **2022**, *16*, 4426.
- [17] A. Huppertsberg, L. Kaps, Z. Zhong, S. Schmitt, J. Stickdorn, K. Deswarte, F. Combes, C. Czysch, J. De Vrieze, S. Kasmi, N. Choteschovsky, A. Klefenz, C. Medina-Montano, P. Winterwerber, C. Chen, M. Bros, S. Lienenklaus, N. N. Sanders, K. Koynov, D. Schuppan, B. N. Lambrecht, S. A. David, B. G. De Geest, L. Nuhn, *J. Am. Chem. Soc.* **2021**, *143*, 9872.
- [18] L. Nuhn, S. De Koker, S. Van Lint, Z. Zhong, J. P. Catani, F. Combes, K. Deswarte, Y. Li, B. N. Lambrecht, S. Lienenklaus, N. N. Sanders, S. A. David, J. Tavernier, B. G. De Geest, *Adv. Mater.* **2018**, *30*, 1803397.
- [19] S. Spranger, M. Javorovic, M. Bürdek, S. Wilde, B. Mosetter, S. Tippmer, I. Bigalke, C. Geiger, D. J. Schendel, B. Frankenberger, *J. Immunol.* **2010**, *185*, 738.
- [20] K. B. Gorden, K. S. Gorski, S. J. Gibson, R. M. Kedl, W. C. Kieper, X. Qiu, M. A. Tomai, S. S. Alkan, J. P. Vasilakos, *J. Immunol.* **2005**, *174*, 1259.
- [21] N. Vanparijs, R. De Coen, D. Laplace, B. Louage, S. Maji, L. Lybaert, R. Hoogenboom, B. G. De Geest, *Chem. Commun.* **2015**, *51*, 13972.
- [22] D. J. Dowling, E. A. Scott, A. Scheid, I. Bergelson, S. Joshi, C. Pietrasanta, S. Brightman, G. Sanchez-Schmitz, S. D. Van Haren, J. Ninković, D. Kats, C. Guiducci, A. De Titta, D. K. Bonner, S. Hirotsue, M. A. Swartz, J. A. Hubbell, O. Levy, *J. Allergy Clin. Immunol.* **2017**, *140*, 1339.
- [23] L. Bixenmann, J. Stickdorn, L. Nuhn, *Polym. Chem.* **2020**, *11*, 2441.
- [24] K. Fukushima, *Biomater. Sci.* **2015**, *4*, 9.
- [25] Y. Dai, X. Zhang, *Polym. Chem.* **2017**, *8*, 7429.
- [26] B. Amsden, *Macromol. Biosci.* **2021**, *21*, 2100085.
- [27] G. Becker, F. R. Wurm, *Chem. Soc. Rev.* **2018**, *47*, 7739.
- [28] S. Kasmi, B. Louage, L. Nuhn, G. Verstraete, S. Van Herck, M. J. Van Steenbergen, C. Vervaet, W. E. Hennink, B. G. De Geest, *Polym. Chem.* **2017**, *8*, 6544.
- [29] S. Kasmi, B. Louage, L. Nuhn, A. Van Driessche, J. Van Deun, I. Karalic, M. Risseeuw, S. Van Calenbergh, R. Hoogenboom, R. De Rycke, O. De Wever, W. E. Hennink, B. G. De Geest, *Biomacromolecules* **2016**, *17*, 119.
- [30] S. Mohajeri, F. Chen, M. De Prinse, T. Phung, J. Burke-Kleinman, D. H. Maurice, B. G. Amsden, *Mol. Pharmaceutics* **2020**, *17*, 1363.
- [31] R. P. Brannigan, A. P. Dove, *Biomater. Sci.* **2017**, *5*, 9.
- [32] X. Wang, J. Wilhelm, W. Li, S. Li, Z. Wang, G. Huang, J. Wang, H. Tang, S. Khorsandi, Z. Sun, B. Evers, J. Gao, *Nat. Commun.* **2020**, *11*, 5828.
- [33] W. Lu, F. Li, R. I. Mahato, *J. Pharm. Sci.* **2011**, *100*, 2418.
- [34] F. Li, M. Danquah, R. I. Mahato, *Biomacromolecules* **2010**, *11*, 2610.
- [35] X. Ke, D. J. Coady, C. Yang, A. C. Engler, J. L. Hedrick, Y. Y. Yang, *Polym. Chem.* **2014**, *5*, 2621.
- [36] A. Das, P. Theato, *Chem. Rev.* **2016**, *116*, 1434.
- [37] M. Scherger, H. J. Räder, L. Nuhn, *Macromol. Rapid Commun.* **2021**, *42*, 2000752.
- [38] H. Guan, Z. Xie, Z. Tang, X. Xu, X. Chen, X. Jing, *Polymer* **2005**, *46*, 2817.
- [39] B. Hassannia, B. Wiernicki, I. Ingold, F. Qu, S. Van Herck, Y. Y. Tyurina, H. Bayır, B. A. Abhari, J. P. F. Angeli, S. M. Choi, E. Meul, K. Heyninck, K. Declerck, C. S. Chirumamilla, M. Lahtela-Kakkonen, G. Van Camp, D. V. Krysko, P. G. Ekert, S. Fulda, B. G. De Geest, M. Conrad, V. E. Kagan, W. V. Berghe, P. Vandenabeele, T. V. Berghe, *J. Clin. Invest.* **2018**, *128*, 3341.
- [40] A. Ahmad, P. Dandawate, S. Schrufer, S. Padhye, F. H. Sarkar, R. Schober, B. Biersack, *Chem. Biodivers.* **2019**, *16*, e1900028.
- [41] Y. Shi, R. Van Der Meel, B. Theek, E. O. Blenke, E. H. E. Pieters, M. H. A. M. Fens, J. Ehling, R. M. Schiffelers, G. Storm, C. F. Van Nostrum, T. Lammers, W. E. Hennink, *ACS Nano* **2015**, *9*, 3740.
- [42] Y. Shi, M. J. Van Steenbergen, E. A. Teunissen, L. Novo, S. Gradmann, M. Baldus, C. F. Van Nostrum, W. E. Hennink, *Biomacromolecules* **2013**, *14*, 1826.
- [43] H. Maeda, *J. Pers. Med.* **2021**, *11*, 229.
- [44] K. Rausch, A. Reuter, K. Fischer, M. Schmidt, *Biomacromolecules* **2010**, *11*, 2836.
- [45] L. Evensen, P. L. Johansen, G. Koster, K. Zhu, L. Herfindal, M. Speth, F. Fenaroli, J. Hildahl, S. Bagherifam, C. Tulotta, L. Prasmickaite, G. M. Mælandsmo, E. Snaar-Jagalska, G. Griffiths, *Nanoscale* **2016**, *8*, 862.
- [46] F. Fenaroli, U. Repnik, Y. Xu, K. Johann, S. Van Herck, P. Dey, F. M. Skjeldal, D. M. Frei, S. Bagherifam, A. Kocere, R. Haag, B. G. De Geest, M. Barz, D. G. Russell, G. Griffiths, *ACS Nano* **2018**, *12*, 8646.
- [47] S. Sieber, P. Grossen, J. Bussmann, F. Campbell, A. Kros, D. Witzigmann, J. Huwyler, *Adv. Drug Delivery Rev.* **2019**, *151-152*, 152.
- [48] N.-J. K. Dal, A. Kocere, J. Wohlmann, S. Van Herck, T. A. Bauer, J. Resseguier, S. Bagherifam, H. Hyldmo, M. Barz, B. G. De Geest, F. Fenaroli, *Small* **2020**, *16*, 1906719.
- [49] J. H. Jung, M. Ree, H. Kim, *Catal. Today* **2006**, *115*, 283.
- [50] Z. Zhang, R. Kuijter, S. K. Bulstra, D. W. Grijpma, J. Feijen, *Biomaterials* **2006**, *27*, 1741.
- [51] J. Kockelmann, J. Stickdorn, S. Kasmi, J. De Vrieze, M. Pieszka, D. Y. W. Ng, S. A. David, B. G. De Geest, L. Nuhn, *Biomacromolecules* **2020**, *21*, 2246.
- [52] S. Van Herck, K. Deswarte, L. Nuhn, Z. Zhong, J. P. P. Catani, Y. Li, N. N. Sanders, S. Lienenklaus, S. De Koker, B. N. Lambrecht, S. A. David, B. G. De Geest, *J. Am. Chem. Soc.* **2018**, *140*, 14300.
- [53] B. Wang, S. Van Herck, Y. Chen, X. Bai, Z. Zhong, K. Deswarte, B. N. Lambrecht, N. N. Sanders, S. Lienenklaus, H. W. Scheeren, S. A. David, F. Kiessling, T. Lammers, B. G. De Geest, Y. Shi, *J. Am. Chem. Soc.* **2020**, *142*, 12133.
- [54] G. M. Lynn, R. Laga, P. A. Darrah, A. S. Ishizuka, A. J. Balaci, A. E. Dulcey, M. Pechar, R. Pola, M. Y. Gerner, A. Yamamoto, C. R. Buechler, K. M. Quinn, M. G. Smelkinson, O. Vanek, R. Cawood, T. Hills, O. Vasalatiy, K. Kastenmüller, J. R. Francica, L. Stutts, J. K. Tom, K. Ah Ryu, A. P. Esser-Kahn, T. Etrych, K. D. Fisher, L. W. Seymour, R. A. Seder, *Nat. Biotechnol.* **2015**, *33*, 1201.
- [55] V. Durai, K. M. Murphy, *Immunity* **2016**, *45*, 719.
- [56] F. Fallarino, C. Orabona, C. Vacca, R. Bianchi, S. Gizzi, C. Asselin-Paturel, M. C. Fioretti, G. Trinchieri, U. Grohmann, P. Puccetti, *Int. Immunol.* **2005**, *17*, 1429.
- [57] S. Wirtz, C. Becker, M. C. Fantini, E. E. Nieuwenhuis, I. Tubbe, P. R. Galle, H.-J. Schild, M. Birkenbach, R. S. Blumberg, M. F. Neurath, *J. Immunol.* **2005**, *174*, 2814.